



On the Role of the Hot Feedback Mode in Active Galactic Nuclei Feedback in an Elliptical Galaxy

Doosoo Yoon^{1,2} , Feng Yuan^{1,3} , Jeremiah P. Ostriker^{4,5} , Luca Ciotti⁶ , and Bocheng Zhu¹

¹ Key Laboratory for Research in Galaxies and Cosmology, Shanghai Astronomical Observatory, Chinese Academy of Sciences, 80 Nandan Road, Shanghai 200030, People's Republic of China; d.yoon@uva.nl, fyuan@shao.ac.cn

² Anton Pannekoek Institute for Astronomy, University of Amsterdam, Science Park 904, 1098 XH Amsterdam, The Netherlands

³ School of Astronomy and Space Science, University of Chinese Academy of Sciences, 100049, Beijing, People's Republic of China

⁴ Department of Astronomy, Columbia University, 550 W. 120th Street, New York, NY 10027, USA

⁵ Department of Astrophysical Sciences, Princeton University, Princeton, NJ 08544, USA

⁶ Department of Physics and Astronomy, University of Bologna, via Piero Gobetti 93/2, I-40129 Bologna, Italy

Received 2019 January 12; revised 2019 September 16; accepted 2019 September 17; published 2019 October 25

Abstract

Depending on the value of the accretion rate, black hole accretion is divided into cold and hot modes. The two modes have distinctly different physics and correspond to two feedback modes. Most previous feedback works focus only on one mode, or the accretion physics is not always properly adopted. Here, by performing hydrodynamical numerical simulations of active galactic nucleus (AGN) feedback in an elliptical galaxy, we show that including both is important, and gives different results from including just one or the other. We specifically focus on the wind and radiation (but neglecting the jet) feedback in the hot mode, to explore whether this particular mode of feedback can play any important feedback role. For this aim, we have run two test models. In one model, we always adopt the cold mode no matter what value the accretion rate is; in another model, we turn off the AGN once it enters into the hot mode. We have calculated the AGN light curves, black hole growth, star formation, and AGN energy duty cycle; and compared the results with the model in which the two modes are correctly included. Important differences are found. For example, if we were to adopt only the cold mode, the total mass of newly formed stars would become two orders of magnitude smaller, and the fraction of energy ejected within the high accretion regime (i.e., $L_{\text{BH}} > 2\%L_{\text{Edd}}$) would be too small to be consistent with observations. We have also investigated the respective roles of wind and radiation in the hot mode.

Key words: accretion, accretion disks – black hole physics – galaxies: active – galaxies: evolution – galaxies: nuclei

1. Introduction

More and more evidence has shown that a supermassive black hole (SMBH) may evolve together with its host galaxy, such as the strong correlation between the mass of the black hole and the luminosity, stellar velocity dispersion, or stellar mass in the galaxy spheroid (Magorrian et al. 1998; Tremaine et al. 2002; see review by Kormendy & Ho 2013). Both observational and theoretical studies now strongly indicate that such a co-evolution between the black hole and the galaxy is the consequence of active galactic nuclei (AGNs) feedback (Di Matteo et al. 2005; Murray et al. 2005; Springel et al. 2005; Croton et al. 2006; Ciotti & Ostriker 2007; Sijacki et al. 2007; Hopkins et al. 2008; Ciotti et al. 2009a; Ostriker et al. 2010; Fabian 2012; Hirschmann et al. 2014; King & Pounds 2015; Naab & Ostriker 2017; Weinberger et al. 2018). In this process, the outputs from the AGN, namely radiation, wind, and jet, interact with the interstellar medium (ISM) in the host galaxy and alter the density and temperature. Consequently, star formation activity is changed, and thus galaxy evolution is affected. The change of the properties of ISM will in turn affect the fueling of the AGN and the evolution of the black hole mass. In this scenario, the value of AGN accretion rate and the model of accretion physics are of central importance for evaluating the effects of AGN feedback because they determine the magnitude of AGN outputs.

Black hole accretion comes in two different modes, namely cold and hot modes, depending on the value of the mass accretion rate of the central black hole. The boundary between

the two modes is $\sim 2\%L_{\text{Edd}}$ (Yuan & Narayan 2014). Simulations of AGN feedback have shown that the black hole activity usually oscillates with time, passing through both modes. The cold and hot accretion modes correspond to the cold and hot feedback modes.⁷ In this paper we will focus on the role of hot feedback mode. Many previous studies have taken into account this mode (e.g., Bower et al. 2006; Croton et al. 2006; Sijacki et al. 2007; Ostriker et al. 2010; McNamara & Nulsen 2012; Li & Bryan 2014; Li et al. 2015; Schaye et al. 2015; Guo 2016; McAlpine et al. 2017; Weinberger et al. 2017, 2018; Guo et al. 2018; Habouzit et al. 2019). For example, by using a semi-analytical approach, Croton et al. (2006) found that this mode of feedback can provide an efficient source of energy to solve the “cooling flow” problem, the exponential cutoff at the bright end of the galaxy luminosity function, and the increased mean stellar age in massive elliptical galaxies. In the hydrodynamical simulation work of Sijacki et al. (2007), they included both the cold and hot modes in their “sub-grid” model and applied it to galaxy cluster formation. In a more recent work, by invoking winds launched in the hot mode, Weinberger et al. (2017) found that their cosmological simulation model can overcome some serious problems in previous galaxy formation models and successfully produce red, non-star-forming massive elliptical galaxies, and achieve realistic gas fraction, black hole growth histories, and

⁷ In the literature, the cold mode is also called “quasar” or “radiative” mode, while the hot mode is often called “radio,” “jet,” “kinetic,” or “maintenance” mode.

thermodynamic profiles in large halos. This feedback model was later applied to the cosmological simulation of Illustris-TNG (Weinberger et al. 2018).

Cosmological AGN feedback works focus on very large scales, so they can simulate the formation and evolution of numerous galaxies. But their resolution has to be rather low, e.g., several kpc; it is thus difficult to study the details of AGN feedback. Another approach is to focus on the much smaller galaxy scale (Ciotti & Ostriker 1997, 2001, 2007; Novak et al. 2011, 2012; Gaspari et al. 2013; Gan et al. 2014; Hopkins et al. 2016; Ciotti et al. 2017; Li et al. 2018; Yoon et al. 2018; Yuan et al. 2018b). The advantage of this kind of model is that we can easily resolve the boundary of black hole accretion flow, i.e., the Bondi radius, which is typically several tens of pc. In this case, the accretion rate can be reliably calculated, so we can avoid the uncertainty as large as ~ 100 or even larger in cosmological simulations (Ciotti & Pellegrini 2017, 2018; Negri & Volonteri 2017). Moreover, we can carefully investigate the details of the AGN feedback, i.e., how the AGN outputs interact with the ISM. This is the approach adopted in the present work.

An equally important issue for the AGN feedback study, in addition to the precise determination of the mass accretion rate, is the AGN physics, which describes the output from the AGN for a given accretion rate. After several decades of observational and theoretical efforts, we now have accumulated quite solid knowledge of black hole accretion (see reviews by Pringle 1981; Blaes 2014; Yuan & Narayan 2014). Based on this knowledge, Yuan et al. (2018b, hereafter Yuan18) have presented a model framework of AGN feedback study by incorporating state-of-the-art AGN physics. This framework has been adopted in several later works of a series (Li et al. 2018; Yoon et al. 2018; Gan et al. 2019), and these works focus on developing different aspects of the model: Yoon et al. (2018) has extended the low angular momentum galaxy in Yuan18 to the case of high angular momentum; Li et al. (2018) has compared the different roles played by AGN feedback and various components of stellar feedback (supernovae and stellar wind); while Gan et al. (2019) has focused on the role of gravitational instability of the galactic circumnuclear, cold gas disk.

One crucial point of the accretion physics is that the radiation and wind outputs from the AGN are distinctly different in the two modes, and they cannot be described by the same scaling. Roughly speaking, both the radiation and wind outputs would be significantly overestimated in the hot mode if we were to choose the scaling of the cold mode. However, most current AGN feedback works focus on either cold mode or hot mode. Even if they include both, the accretion physics, especially the physics of the hot mode, is not correctly adopted, because they often adopt the same scaling for the wind and radiation outputs as the cold mode, which is incorrect.

In this paper, we show how important it is to include both modes by performing high-resolution hydrodynamical simulations following Yuan18. We specifically focus on the roles of wind and radiation feedback in the hot mode.⁸ Both observational and theoretical simulations have shown that the AGNs reside in the hot mode for a much longer time than in the cold mode (e.g., Haiman & Hui 2001; Heckman et al. 2004; Greene & Ho 2007; Kauffmann & Heckman 2009;

Shankar et al. 2010; Yuan18; Yoon et al. 2018; Gan et al. 2019). For instance, a statistical study has shown that the percentage of the time spent in the active phase of the black hole, which roughly corresponds to the cold accretion mode, is reported to be $\sim 0.4\%$ or even smaller (Greene & Ho 2007). Therefore, although the wind and radiation in the hot mode are much weaker than those in the cold mode, it is hard to exclude the possibility that the hot mode feedback still plays an important role due to its cumulative effects.

This paper is structured as follows. In Section 2, we overview different components of our model, including the simulation setup, the galaxy model we adopt, the calculations of star formation rate, the stellar feedback, and the physics of cold and hot accretion modes. In Section 3, we describe our simulation results. We summarize our results in Section 4.

2. Model

The code that this work will be based on is called “*MACER*,” which has been described in Yuan18 (see also Yuan et al. 2018a for a short description of the main components of the model) and is based on the code originally developed by Ciotti & Ostriker (1997, 2001, 2007) over several years. Specifically, using this code, we study the AGN feedback in an isolated elliptical galaxy. The Bondi radius is resolved and thus the accretion rate can be calculated precisely. We then calculate the AGN outputs including the wind and radiation based on the sub-grid accretion physics; the interaction of radiation and wind with the interstellar medium is also calculated by considering simplified radiative transfer. Other physical processes such as star formation and energy release through stellar evolution, including supernovae (SNe) Types I and II, are taken into account in a way we will describe in the following sections. Importantly, we also include the very significant mass input to the ISM from planetary nebulae and asymptotic giant branch stars. For the convenience of the readers, in the following sections we summarize the key components of the model.

2.1. Simulation Setup

Simulations were performed with the parallel ZEUS-MP/2 code (Hayes et al. 2006) using axisymmetric spherical coordinates (r, θ) . The black hole is located at the origin. We adopt a logarithmic mesh with 120 grids in the radial direction, which covers the range of 2.5 pc–250 kpc. We use the standard “outflow boundary condition” in the inner and outer radial boundary. In θ direction, 30 grids are uniformly divided. The highest resolution is thus achieved at the innermost region, which is ~ 0.3 pc. Such a configuration is essential, because the innermost region is the place where the radiation and the wind originate and where the accretion rate of the black hole is determined, and thus are most important for AGN feedback. Even for the hot gas in the galactic center region, the Bondi radius is ~ 6 pc; for the cold gas, the Bondi radius is much larger (Yuan18). So the inner boundary of our simulation domain is at least two times smaller than the Bondi radius. This means that we can precisely calculate rather than estimate the black hole accretion rate, which is crucial to evaluate the effects of the feedback.

Within the inner boundary, the accretion flow still cannot be resolved. We treat the accretion process in that region as sub-grid physics. We describe this part in Section 2.4 (see also, Yuan18).

⁸ We neglect the jet in our model; we will discuss this issue further in Section 2.4.

2.2. Galaxy Model

In this work, we focus on the secular evolution of an isolated elliptical galaxy. We only consider the gas produced by the stellar evolution as the material for black hole accretion. In reality, there must be some external gas supply to the galaxy. One is the cosmological inflow from intergalactic medium. In addition, for those galaxies located at the center of galaxy clusters or galaxy groups, there will be an enormous potential supply of gas from their gaseous halo, the infall of which causes the cooling flow problem. Because of these limitations, our present work provides a necessary (but not sufficient) condition for AGN feedback to be important for the quenching of galaxies. And last, mergers are also neglected. We make this assumption because the majority of nuclear activity in the universe has taken place due to internal dynamical instabilities rather than violent mergers (Cisternas et al. 2011). Observations indicate that, at least for moderate-luminosity AGNs, the growth of the black hole and star-forming galaxies has been regulated dominantly by internal secular processes (Kocevski et al. 2012; Fan et al. 2014). But galaxy merger processes may still be effective in fueling gas to the central black hole (Mihos & Hernquist 1996; Di Matteo et al. 2005). We will study the effect of including external gas supply and galaxy merger in our future work.

In our simulation, we start with very low gas density in the galaxy as an initial condition. Over a cosmological time, the total mass loss from the passively evolving stars in elliptical galaxies can reach up to $\sim 20\%$ of the initial stellar mass (Ciotti & Ostriker 2012), mainly by red giant winds and planetary nebulae. This is two orders of magnitude larger than the mass of the initial central black hole. If all of this gas was accreted into the black hole, the mass of the hole would be ~ 100 times larger than what is observed, $M_{\text{BH}} \simeq 10^{-3} M_{\star}$ (e.g., Magorrian et al. 1998; Kormendy & Ho 2013). Again, we leave the study of including additional initial gas in the galaxy to a future work.

Following Ciotti et al. (2009b), we adopt the Jaffe (1983) profile for the initial stellar distribution,

$$\rho_{\star} = \frac{M_{\star} r_{\star}}{4\pi r^2 (r_{\star} + r)^2}, \quad (1)$$

where M_{\star} is the total stellar mass and is set to be $M_{\star} = 3 \times 10^{11} M_{\odot}$, and $r_{\star} = 6.9$ kpc is the scale length of the galaxy, which corresponds to the projected half-mass radius of $R_e = 5.14$ kpc. The migration of stars is not taken into account in our simulation; instead, both the initial stars and the newly born stars keep their locations all of the time.

Along with the central black hole, the dark matter halo and a stellar spheroid are considered as the dominant contributors of the gravitational potential in the galaxy. The self-gravity of the ISM is ignored in our simulation. The density profile of the dark matter halo is assumed to be spherically symmetric. The total mass profile (dark matter plus stars) decreases as r^{-2} , as observed (e.g., Rusin & Kochanek 2005; Czoske et al. 2008; Dye et al. 2008). To simplify our problem, we further assume that the stars rotate slowly. Because the gas in our simulation comes from the evolving stars, this means that the specific angular momentum of the gas is small, and we do not need to deal with the angular momentum transfer. For the case of high angular momentum, readers can refer to Yoon et al. (2018) and Gan et al. (2019).

And last, the initial black hole mass is set by the empirical correlation between the black hole mass and the stellar mass given in Kormendy & Ho (2013), which for the adopted galaxy model gives $M_{\text{BH,init}} = 1.8 \times 10^9 M_{\odot}$.

2.3. Star Formation and Stellar Feedback

The cold gas reservoir in the central galaxy is an ideal place for the onset of the radiative cooling instability, which leads to active star formation. We calculate the star formation rate per unit volume by means of a recipe that reproduces quite well the standard Schmidt–Kennicutt empirical relation, as in our previous works (e.g., Novak et al. 2011; Yuan et al. 2018b),

$$\dot{\rho}_{\text{SF}} = \frac{\eta_{\text{SF}} \rho}{\tau_{\text{SF}}}, \quad (2)$$

where η_{SF} is the star formation efficiency and τ_{SF} is the star formation timescale,

$$\tau_{\text{SF}} = \max(\tau_{\text{cool}}, \tau_{\text{dyn}}), \quad (3)$$

where the cooling timescale and the dynamical timescale are,

$$\tau_{\text{cool}} = \frac{E}{C}, \quad \tau_{\text{dyn}} = \min(\tau_{\text{ff}}, \tau_{\text{rot}}) \quad (4)$$

with

$$\tau_{\text{ff}} = \sqrt{\frac{3\pi}{32G\rho}}, \quad \tau_{\text{rot}} = \frac{2\pi r}{v_k(r)} \quad (5)$$

where E is the internal energy density, C is the effective radiative cooling rate per unit volume, G is the Newtonian gravitational constant, and $v_k(r)$ is the Keplerian velocity at radius r . The radiative cooling rate C is computed by using the formulae in Sazonov et al. (2005). It describes the net heating/cooling rate in photoionization equilibrium with a radiation field corresponding to the average quasar spectral energy distribution. In particular, line and continuum heating/cooling, bremsstrahlung losses, and Compton heating/cooling are taken into account. We note that for simplicity we have ignored the chemical evolution of ISM and the existence of the dust in the galaxy, which can affect the star formation process.

Different from our previous works (e.g., Yuan18), which only adopted the previously mentioned standard Schmidt–Kennicutt prescription to calculate the star formation rate, in the present work we add the following additional constraints. That is, we do not allow star formation when the gas temperature is higher than 4×10^4 K, nor when the density is lower than 1 cm^{-3} . This is to mimic the fact that stars are formed from cold and dense molecular gas. In addition, we now choose a lower value of the star formation efficiency. Yuan18 adopt $\eta_{\text{SF}} = 0.1$ while $\eta_{\text{SF}} = 0.01$ is adopted in the present work.

The calculation of stellar evolution in our simulation follows the description presented in Ciotti & Ostriker (2012). Both the stellar winds and SN explosions will provide sources of mass and energy to the galaxy, and these effects will be taken into account in our simulations. This gas, when it cools due to radiation, can form stars. Some newly formed massive stars evolve quickly and explode via SNe II. They will then eject mass and energy into the ISM at some rates, and this has also been considered in our simulation.

2.4. Physics of the Cold and Hot Accretion Modes

Depending on the value of the mass accretion rate, black hole accretion has two sets of solutions. When the accretion rate is higher than $\sim 2\% \dot{M}_{\text{Edd}}$, here the Eddington accretion rate $\dot{M}_{\text{Edd}} \equiv 10L_{\text{Edd}}/c^2$, the accretion is in the cold mode, because the temperature of the accretion flow is relatively low; when the accretion rate is lower than this value, the accretion will be in the hot mode, because the temperature of the accretion flow is several orders of magnitude higher, nearly virial.⁹ The representative solutions in the cold and hot modes are the standard thin disk solution (Shakura & Sunyaev 1973) and the advection-dominated accretion flow (ADAF; Narayan & Yi 1995; Yuan & Narayan 2014).

The threshold of $2\% \dot{M}_{\text{Edd}}$ applies to the accretion rate in the innermost region of the accretion flow, which is usually smaller than the rate at the inner boundary of the simulation domain R_{in} , partly because of the existence of wind within the accretion flow. However, in our model we directly use the threshold of $2\% \dot{M}_{\text{Edd}}$ at R_{in} to discriminate between the two modes. This is because the wind is weak close to or above this accretion rate, as we will see later in this section.

Because we cannot resolve the scale within R_{in} , we have to use some sub-grid physics. When the accretion is in the cold mode, the gas will first freely fall until a small accretion disk is formed with the size of the circularization radius. The accretion rate close to the black hole is calculated based on this scenario. Readers can refer to Section 2.2.1 of Yuan18 for details of the calculation. When the accretion is in the hot mode, the accretion flow will be in the form of a thin disk at large radii; at a certain radius, R_{tr} , the thin disk will be truncated and transit into a hot accretion flow (Yuan & Narayan 2014).

Based on this scenario, once we have obtained the accretion rate at R_{in} , we can calculate the outputs from the AGN based on our knowledge of black hole accretion. The outputs in general include radiation, wind, and a jet. In the present work, we only consider wind and radiation, and neglect the jet. This is partly because, although jet feedback is generally believed to play an important role on the galaxy cluster scale (but different opinions still exist, e.g., Vernaleo & Reynolds 2006; Guo 2016; Guo et al. 2018), no consensus has been reached about whether the jet is important on the galaxy scale. This is because, although jets can be very powerful because they are well collimated, they may just pierce through the galaxy without depositing significant energy in the ISM. In addition, it is still an open question which one, wind or jet, is more powerful. Theoretically, in the case of a non-spinning black hole, Yuan et al. (2015) has shown that both the energy and momentum fluxes of wind are significantly larger than jet.¹⁰ But in the case of a rapidly spinning black hole, the jet may become significantly stronger than winds due to the additional powering of jet by the rotating black hole (H. Yang et al. 2019, in preparation). Moreover, it is unlikely that the black hole spin is perfectly aligned with the angular momentum of the accretion disk, resulting in a precessing jet (Falceta-Gonçalves et al. 2010). Such a precession may help the interaction

between jet and ISM. We will investigate the role of jet in the future.

The dynamics of the accretion flow and wind in the cold and hot modes are very different (Yuan & Narayan 2014). For the wind in the cold mode, three mechanisms have been proposed for the formation of wind, namely thermal, radiation line force, and magnetic field. But because of the technical difficulties, theoretical works usually focus only on one mechanism, and so far no consensus has been reached as to the dominant mechanism of wind formation. On the observational side, however, we have accumulated abundant observational data on winds (e.g., Crenshaw et al. 2003; Arav et al. 2008; Tombesi et al. 2012; King & Pounds 2015). Following Yuan18, in the present work we adopt the statistical results of wind properties obtained in Gofford et al. (2015), which are obtained by fitting the observations of the wind from 51 AGNs observed by *Suzaku*. The mass flux and velocity of wind are found to be a function of the AGN bolometric luminosity L_{bol} , described by the following equations,

$$\dot{M}_{\text{w,c}} = 0.28 \left(\frac{L_{\text{bol}}}{10^{45} \text{ erg s}^{-1}} \right)^{0.85} M_{\odot} \text{ yr}^{-1}, \quad (6)$$

$$v_{\text{w,c}} = 2.5 \times 10^4 \left(\frac{L_{\text{bol}}}{10^{45} \text{ erg s}^{-1}} \right)^{0.4} \text{ km s}^{-1}. \quad (7)$$

We set the largest velocity of the wind to be 10^5 km s^{-1} . But we would like to emphasize that a large degree of diversity of wind properties exists in different observational results. The effect of wind parameters on AGN feedback will be investigated in our next work (Z. Yao et al. 2019, in preparation).

As for the angular distribution of the mass flux of wind from the cold disk, following our previous works (e.g., Yuan18), we simply assume that the mass flux of wind $\propto \cos(\theta)$, implying that the wind is strongest toward the polar region. This is in rough accord with the observational prevalence of BAL winds for roughly one-third of active AGNs (Arav et al. 2008). We note that because our galaxy model is almost spherically symmetric, the orientation of the wind is not important.

The bolometric luminosity from the cold accretion flow is described by

$$L_{\text{bol,cold}} = L_{\text{BH,cold}} = \epsilon_0 \dot{M}_{\text{BH,cold}} c^2 \text{ erg s}^{-1}; \quad (8)$$

here the radiative efficiency $\epsilon_0 = 0.1$ and $\dot{M}_{\text{BH,cold}}$ is the mass accretion rate at the black hole horizon. In our model, we assume the radiation for both cold and hot modes are isotropic and ISM is optically thin when we calculate the radiative transfer. The dust is ignored in our model, although it may dominate the radiation pressure in some regions of the galaxy. The Compton heating and cooling are calculated in terms of ‘‘Compton temperature’’ T_{C} , which represents the energy-weighted average energy of photons emitted by the AGN. For the cold mode, $T_{\text{C,cold}} = 2 \times 10^7 \text{ K}$ (Sazonov et al. 2004).

The character of the study of wind in the hot mode is quite different compared with the cold mode. It is much more difficult to detect wind in the hot mode. One reason is the dimness of the sources hosting hot accretion flows. Another reason is that the temperature of wind in the hot mode is too high, thus the wind is usually fully ionized; it is therefore difficult to produce any line features. Consequently, although

⁹ In fact, theoretically the cold mode solution may still exist when the accretion rate is lower than $2\% \dot{M}_{\text{Edd}}$. However, observations of black hole X-ray binaries show that in this case only the hot mode accretion can be realized in nature (McClintock & Remillard 2006; Yuan & Narayan 2014). This is called ‘‘strong ADAF principle’’ in Narayan & Yi (1995).

¹⁰ In the case of a non-spinning black hole, jet can still be powered by the rotating accretion flow (Yuan et al. 2015).

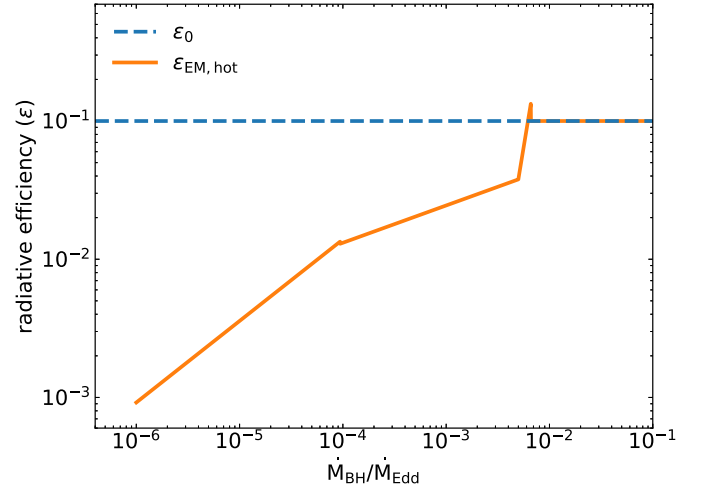
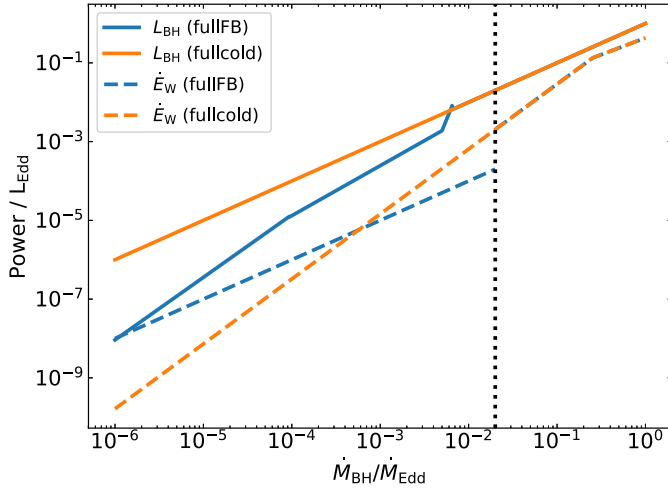


Figure 1. *Left:* the comparison of AGN luminosity and kinetic power as a function of accretion rate between the fullFB model and fullcoldFB model. *Right:* the radiative efficiency for the cold mode (ϵ_0 , dashed blue line) and the hot mode ($\epsilon_{\text{EM,hot}}$, solid orange line) as a function of accretion rate.

we are gradually accumulating more and more observational evidences for the existence of wind in hot accretion flows (e.g., Wang et al. 2013; Tombesi et al. 2014; Cheung et al. 2016; Homan et al. 2016; Ma et al. 2018), the observational data are so far not good enough to constrain the properties of wind, as in the case of cold mode. For example, in Wang et al. (2013), by modeling the iron emission line profile, we obtain the radial density profile of the hot accretion flow around the SMBH in our galactic center, from which we infer the existence of wind. In another example, Cheung et al. (2016) detect bisymmetric emission line structure in the polar direction of a low-luminosity AGN, from which they can measure the spatial distribution of velocity field of the emission clouds. They infer the existence of wind by explaining such a velocity field.

The relevant study starts from the pioneer hydrodynamical simulation work by Stone et al. (1999), followed by both analytical works and hydrodynamical and magneto-hydrodynamical numerical simulations (e.g., Narayan et al. 2012; Yuan et al. 2012a, 2012b, 2015; Li et al. 2013; Sądowski et al. 2013; Bu et al. 2016a, 2016b; Mosallanezhad et al. 2016; Bu & Mosallanezhad 2018). Different from the wind from cold mode, theoretical study of wind from hot mode is much easier. On the one hand, radiation can be neglected for wind study in the hot mode. On the other hand, it is much easier to simulate a geometrically thick accretion flow than a thin disk. In spite of these, the study of the wind properties in the hot mode is not trivial, because one has to face the challenge of how to discriminate winds (i.e., “real outflow”) from turbulence (see discussions in Stone et al. 1999).

By applying the “virtual particle trajectory” approach and based on three-dimensional general relativistic magnetohydrodynamic simulation, Yuan et al. (2015) successfully overcome this difficulty and calculate the wind properties, including mass flux, velocity, and spatial distribution:

$$\dot{M}_{\text{W,H}} \approx \dot{M}(R_{\text{in}}) \left[1 - \left(\frac{3 r_s}{r_{\text{tr}}} \right)^{0.5} \right], \quad (9)$$

$$v_{\text{W,H}} \approx (0.2 - 0.4) v_{\text{K}}(r_{\text{tr}}), \quad (10)$$

where $r_s \equiv 2GM_{\text{BH}}/c^2$ is the Schwarzschild radius, v_{K} is the Keplerian velocity, and r_{tr} is the truncation radius of the outer thin disk described by Yuan & Narayan (see 2014, and references therein),

$$r_{\text{tr}} \approx 3 r_s \left[\frac{2 \times 10^{-2} \dot{M}_{\text{Edd}}}{\dot{M}(R_{\text{in}})} \right]^2. \quad (11)$$

In the present work, we will adopt these theoretical results because of our lack of good observational constraints. We emphasize that the aforementioned results only apply to the case of “SANE” (i.e., standard and normal evolution) and a non-spinning black hole. It is necessary to calculate the cases of “MAD” (i.e., magnetically arrested disk) and a spinning black hole (H. Yang et al. 2019, in preparation).

As for the angular distribution of wind from hot accretion flow, based on the detailed analysis presented in Yuan et al. (2015), we set that the mass flux of the wind is distributed mainly within $\theta \sim 30^\circ - 70^\circ$ and $110^\circ - 150^\circ$ above and below the equatorial plane, respectively. We note that the formation of Fermi bubbles detected in the Milky Way has been successfully explained by the interaction between wind launched from the hot accretion flow around Sgr A* and the interstellar medium in the Galaxy (Mou et al. 2014, 2015).

We now calculate the radiation in the hot mode. The black hole accretion rate in the hot mode is

$$\dot{M}_{\text{BH,hot}} \approx \dot{M}(R_{\text{in}}) \left(\frac{3 r_s}{r_{\text{tr}}} \right)^{0.5}. \quad (12)$$

The radiative efficiency of the hot accretion flow is no longer a constant but a function of accretion rate. It is described by the following formula (Xie & Yuan 2012),

$$\epsilon_{\text{EM,hot}}(\dot{M}_{\text{BH}}) = \epsilon_0 \left(\frac{\dot{M}_{\text{BH}}}{0.1 L_{\text{Edd}}/c^2} \right)^a, \quad (13)$$

Table 1
Description of the Models

model	AGN _{cold}	AGN _{hot}
fullFB	yes	yes
fullcoldFB	yes	yes ^a
nohotFB	yes	no
nohotradFB	yes	only AGN _{hot,mech}
nohotmechFB	yes	only AGN _{hot,rad}

Note.

^a In the fullcoldFB model, the radiation and wind outputs of AGN always follow the prescriptions in the cold mode over the entire range of accretion rate.

the values of ϵ_0 and a are given in Xie & Yuan (2012), and we copy them here:

$$(\epsilon_0, a) = \begin{cases} (0.2, 0.59), & \dot{M}_{\text{BH}}/\dot{M}_{\text{Edd}} \lesssim 9.4 \times 10^{-5} \\ (0.045, 0.27), & 9.4 \times 10^{-5} \lesssim \dot{M}_{\text{BH}}/\dot{M}_{\text{Edd}} \lesssim 5 \times 10^{-3} \\ (0.88, 4.53), & 5 \times 10^{-3} \lesssim \dot{M}_{\text{BH}}/\dot{M}_{\text{Edd}} \lesssim 6.6 \times 10^{-3} \\ (0.1, 0), & 6.6 \times 10^{-3} \lesssim \dot{M}_{\text{BH}}/\dot{M}_{\text{Edd}} \lesssim 2 \times 10^{-2}. \end{cases} \quad (14)$$

The comparison of the radiative efficiency between the cold and hot modes has been shown in the right panel of Figure 1. Note that the efficiency of the hot mode is comparable to that of the cold mode when the accretion rate is high. The radiation emitted from a hot accretion flow has relatively more hard photons compared with that from a thin disk; thus, the Compton temperature of a hot accretion flow is higher, $T_{\text{C,hot}} \sim 10^8$ K (Xie et al. 2017). Such a high $T_{\text{C,hot}}$ results in a relatively efficient radiative heating and is likely the reason for the importance of radiative feedback in the hot mode, as we will discuss in Section 3.4.

We note that in the current work we ignore dust in the ISM when we calculate the radiative feedback. If the dust were to be included, the opacity could be orders of magnitude larger than the electron-scattering opacity (e.g., Novak et al. 2012); thus, a much larger portion of radiation could be deposited in the ISM. In this case, as shown by the right plot of Figure 1 in Yuan18, if the AGN accretion rate is not very low, the momentum flux of radiation will be comparable to or even larger than that of the wind. So radiative feedback will be more important than what we show here.

2.5. Models

To investigate the role of the hot mode feedback, in this paper we have produced four models, as given in Table 1. In the model “fullcoldFB,” we assume that the AGN feedback occurs only in cold mode over the entire range of accretion rates. In the model “nohotFB,” when the accretion rate is lower than the “boundary” between the cold and hot modes, instead of adopting the hot mode as in the fullFB model, we simply turn off the AGN; i.e., there will be no radiation and wind at all in this case. We compare the simulation results of these two models with those of the “fullFB” model presented in Yuan18 (but with some improvements as described in Section 3.1). To understand the respective role of radiation and wind in the hot mode, we carry out two additional models without wind

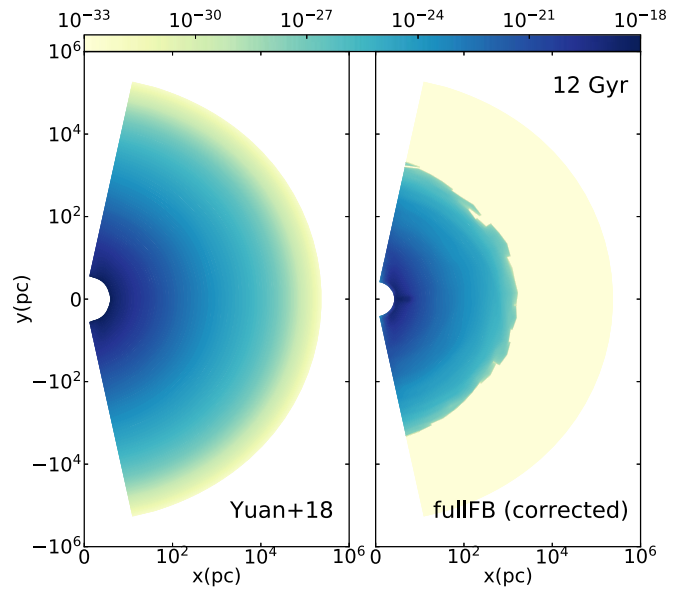


Figure 2. The mass density of the newly born stars, which are integrated for the entire simulation time. Left plot is the result from the fiducial model in Yuan18, and the right plot is the “corrected” result from the present work, at which stars form only when the temperature is below 4×10^4 K and the gas density is higher than 1 cm^{-3} .

(mechanical) feedback (i.e., “nohotmechFB”) and radiative feedback (i.e., “nohotradFB”), respectively.

The left panel of Figure 1 compares the radiation and wind power between the fullFB and fullcoldFB models. The differences are of course only in the regime of $L \lesssim 2 \times 10^{-2} L_{\text{Edd}}$ and they are very significant. Radiation in the fullcoldFB model is almost always stronger than that in the fullFB model. Wind power in the fullcoldFB model is also much stronger than that in the fullFB model unless the luminosity is lower than $\sim 6 \times 10^{-4} L_{\text{Edd}}$. As we will show in Section 3, these differences produce important effects on the AGN feedback.

3. Results

3.1. Some Results of the Updated FullFB Model

For the fullFB model, we employ the AGN feedback for both cold and hot modes as mentioned previously. This model is identical to that in Yuan18 but with two improvements in the present paper. One is on the calculation of star formation, as described in Section 2.3. The effect of adopting the new star formation calculation is shown by Figure 2. We can see that the amount of newly formed stars is significantly reduced compared with Yuan18, and the distribution of the formed stars is highly concentrated within ~ 1 kpc. This is in a good agreement with the recent observation (Tadaki et al. 2018), which showed that a large fraction of stars forms in the central 1 kpc.

In addition to this improvement, we have also corrected a bug in computing the energy flux of the wind for the fullFB model in Yuan18. Although this does not change the overall evolution of the black hole and the galaxy, we do find that it over-produced the wind power. And last, we would like to emphasize that, similar to Yuan18, all models in this work assume only a small degree of galactic rotation; thus, there is no density-enhanced disk (see Yoon et al. 2018, as is the result for the model with higher degree of galactic rotation).

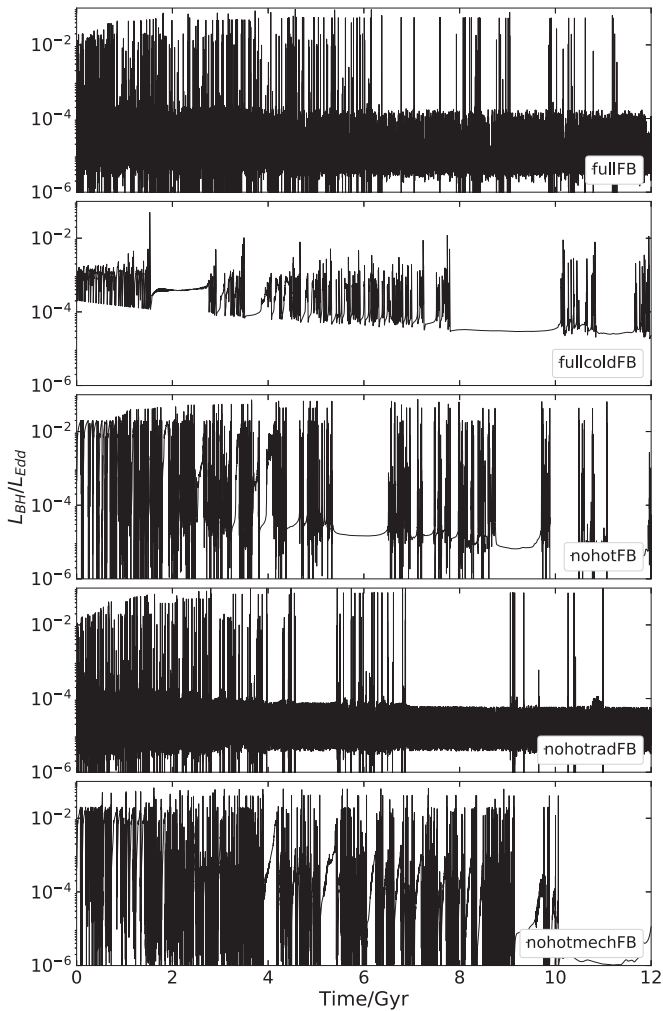


Figure 3. Light curves of AGN luminosity as a function of time for various models.

Figure 3 shows the AGN light curves. We can see that the overall shape is the same as in Yuan18; it stays at low luminosity ($L_{\text{BH}} \sim 10^{-5}L_{\text{Edd}}$) for most of its lifetime, with occasional bursts. These bursts occur more frequently at earlier times as a consequence of the more abundant gas supply. In our galaxy configuration, the initial gas density in the galaxy is very low and the stellar mass loss and SNe Ia are the main feedback for the gas in the galaxy (Pellegrini 2012). Here, according to the stellar population synthesis model that we adopt, most of the stellar mass is lost at early times, resulting in more violent AGN feedback at that stage.

Figure 4 shows the total mass of the gas in the galaxy within different temperature ranges. While most of the gas stays at $T > 10^7$ K, it occasionally becomes cold enough for star formation ($T < 4 \times 10^4$ K) as a consequence of thermal instability (e.g., Li & Bryan 2014; Li et al. 2015).

3.2. Comparison between FullFB and FullcoldFB Models

The resultant light curve for the fullcoldFB model is shown in Figure 3. Compared with the light curve of the fullFB model, we can see several obvious differences. One is that the luminosity of the AGN is always below $10^{-2}L_{\text{Edd}}$ in the fullcoldFB model, while it can be above this value in the fullFB model. The second difference is that we can clearly see a trend

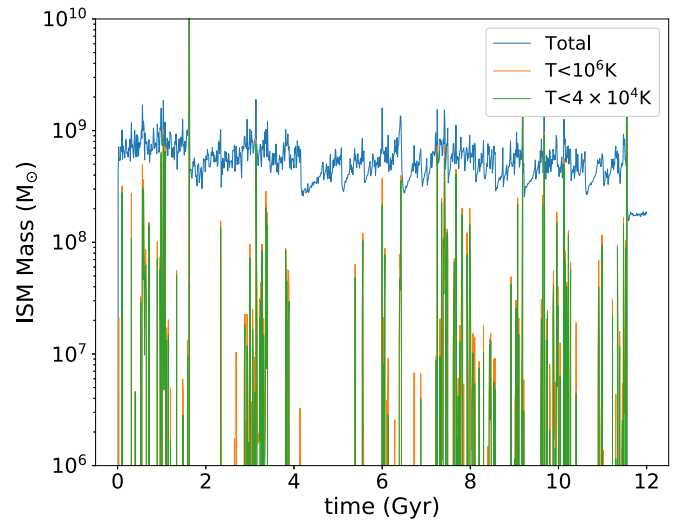


Figure 4. Mass budget of cold and hot ISM in the fullFB model.

of decreasing luminosity with cosmological evolution time in the fullcoldFB model, while it is not so obvious in the fullFB model. The third difference is that the light curve in the fullcoldFB model is much less bursty compared with the fullFB model.

Yuan18 have shown that the AGN accretion rate and light curve are mainly controlled by the wind feedback rather than radiative feedback. So we believe that the former two differences are because of the stronger wind in the fullcoldFB model.¹¹ When the wind becomes stronger, more gas surrounding the black hole will be pushed away and thus the accretion rate will in general become smaller. In addition, more gas will be blown out of the galaxy in the form of galactic wind; thus, the available gas for fueling the black hole will gradually become less. For the third difference between the fullcoldFB and fullFB models mentioned above, we speculate that this is because of the stronger radiation in the fullcoldFB model. The bursty feature of the AGN is likely because of the accretion of small cold clumps by the black hole. The clumps are formed by thermal instability (e.g., McCourt et al. 2012; Sharma et al. 2012; Gaspari et al. 2013; Li & Bryan 2014; Li et al. 2015; Qiu et al. 2018; Wang et al. 2019). When radiation is stronger, radiative heating becomes stronger; thus, it is harder for clumps to form.

Figure 5 shows the evolution of the black hole mass for each model. We can see that the growth of the black hole in both fullFB and fullcoldFB models is very little.

Figure 6 shows the radial mass distribution of newly born stars for various models, which is integrated for the entire simulation time. The results of the fullFB and fullcoldFB models are shown by the thick blue and thick orange lines respectively. It is apparent that star formation is highly suppressed in the fullcoldFB model compared with the fullFB model. The reason for reduced star formation in the fullcoldFB model may be twofold. On the one hand, the AGN radiation is stronger in the fullcoldFB model, resulting in stronger radiative heating to the gas in a large region of the galaxy where the optical depth is smaller than unity (Yuan18). On the other hand, the wind in the fullcoldFB model is also much stronger

¹¹ Although the wind is stronger when $L \lesssim 6 \times 10^{-4}L_{\text{Edd}}$, both the wind mass flux and velocity are very small in that regime (refer to Equations (6) and (7)); thus, its role is not significant compared with the case of $L \gtrsim 6 \times 10^{-4}L_{\text{Edd}}$.

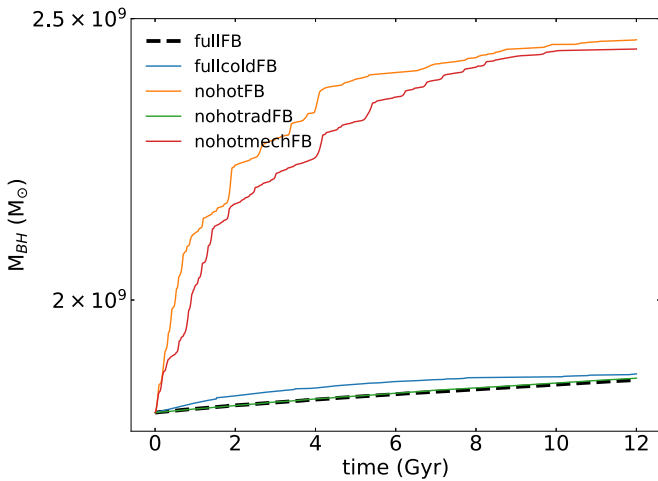


Figure 5. The evolution of black hole mass as a function of time for various models.

than in the fullFB model. The strong wind blows away the gas in the galactic center up to distance of a few kpc, which results in the decrease of density and suppression of star formation. The star formation perhaps can be enhanced temporarily at \sim kpc scale, where the gas is compressed due to the interaction between the wind and the ISM (Cresci et al. 2015). However, such a temporal enhancement is averaged out and not present in this time-integrated figure.

The right panel of Figure 6 shows the total mass of newly born stars for various models. We can see that the total mass of new stars in the fullcoldFB model is an order of magnitude smaller than in the fullFB model.

And last, let us examine the percentage of the emitted total energy above a given Eddington ratio. Figure 7 shows the predicted results for various models. Observationally, it is believed that AGNs spend most of their time in the low-luminosity AGN phase, but emit most of their energy during the high-luminosity AGN phase (Soltan 1982; Yu & Tremaine 2002). For the fullFB mode, the fraction of energy ejected above $2\%L_{\text{Edd}}$ is about 25%.¹² But for the fullcoldFB model, the fraction becomes very small ($\sim 2\%$), inconsistent with observations.

3.3. Comparison between FullFB and NohotFB Models

The AGN light curve produced by the nohotFB model is shown in Figure 3. Unlike the fullFB model, in which the AGN luminosity is $\sim 10^{-5}L_{\text{Edd}}$ most of the time, the AGN luminosity in the nohotFB model becomes generally higher and fluctuates in the range of $10^{-5} \lesssim L_{\text{BH}}/L_{\text{Edd}} \lesssim 10^{-2}$. The higher “average” AGN luminosity is obviously because of the absence of AGN feedback when $L \lesssim 2\%L_{\text{Edd}}$. Due to the absence of wind and radiation, the gas surrounding the black hole has an average higher density and lower temperature, and thus the accretion rate is higher.

In accordance with the AGN light curves, the black hole growth is also distinctly different between the fullFB and nohotFB models, as shown by Figure 5. For the nohotFB model, because the accretion rate is on average significantly higher than in the fullFB model, the black hole can grow to a

larger mass than in the fullFB model. Although the hot mode occurs at low accretion rates, this mode is not negligible, because the time fraction of being in hot mode is very large. This result strongly indicates the importance of including the hot mode feedback.

The radial distribution of newly born stars for the nohotFB model is shown in Figure 6 by the thin green line. Compared with the fullFB model, we can see that in the nohotFB model, the star formation is enhanced within ~ 4 pc, but reduced outside of this radius. In other words, the presence of the wind and radiation in the hot mode suppresses the star formation only in the vicinity of the black hole, which is apparently surprising. Our explanation is as follows. The mechanical feedback by wind (maybe radiation also) pushes gas outward, affecting the star formation activity in a complicated way. On the one hand, the wind can reduce star formation as it depletes the inner region in the galaxy. On the other hand, it can also enhance star formation because it can make the gas inhomogeneous by compressing the gas. The net effect on the total star formation may depend on the power of the wind. If the wind is very powerful, it can push a lot of gas to a large radius, where it is difficult for a star to form because the density is too low. If the wind is weak, it cannot push the gas too far away, and its main role is to make the gas inhomogeneous, thus helping the star formation. Because the wind in the hot mode is somewhat weak, it suppresses the formation only in the small radii (i.e., ≤ 4 pc), where it is still energetic enough to push the gas away. At large radii (i.e., ≥ 4 pc), the gas is just perturbed by the wind but not pushed away; thus, star formation is enhanced. As we can see in the right panel of Figure 6, the total mass of newly born stars in the nohotFB model is smaller than in the fullFB model. We note that the wind in the cold mode is powerful enough to push the gas to large radius, where star formation is hard because the density is too low, so wind in the cold mode always suppresses star formation.

The percentage of the total energy emitted above a given value of Eddington ratio for the nohotFB model is shown in Figure 7. We can see that, similar to the case of the fullcoldFB model, the percentage of energy emitted above $2\%L_{\text{Edd}}$ for nohotFB model is very small, $\sim 1\%$, which is inconsistent with the observations. This again indicates that the hot feedback mode is important.

3.4. The Roles of Radiation and Wind in the Hot Feedback Mode

We have also run two additional models to study the roles of radiation and wind in the hot mode, i.e., the nohotradFB model and nohotmechFB model. We find that the overall results of the nohotradFB model are mostly the same as the fullFB model. This implies that, in the low accretion regime, the mechanical feedback is likely dominant over the radiative feedback.

For the nohotmechFB model, we find that the AGN luminosity light curve and star formation activity have similar shapes with the nohotFB model, which can also be explained by the dominance of mechanical feedback in the hot mode. However, we find that the black hole growth is more suppressed in the nohotmechFB model compared with the nohotFB model. This is likely because radiation in the hot feedback mode can heat the gas surrounding the black hole, thus reducing the mass accretion rate of the black hole. This indicates that, depending on the physical questions of interest, radiation in the hot mode still can play an important role and cannot be neglected.

¹² This value is larger than that given in Yuan18, which was only 6%, and is more consistent with the observational constraints. Such a difference is likely because of the two updates of our model we have mentioned in Section 3.1.

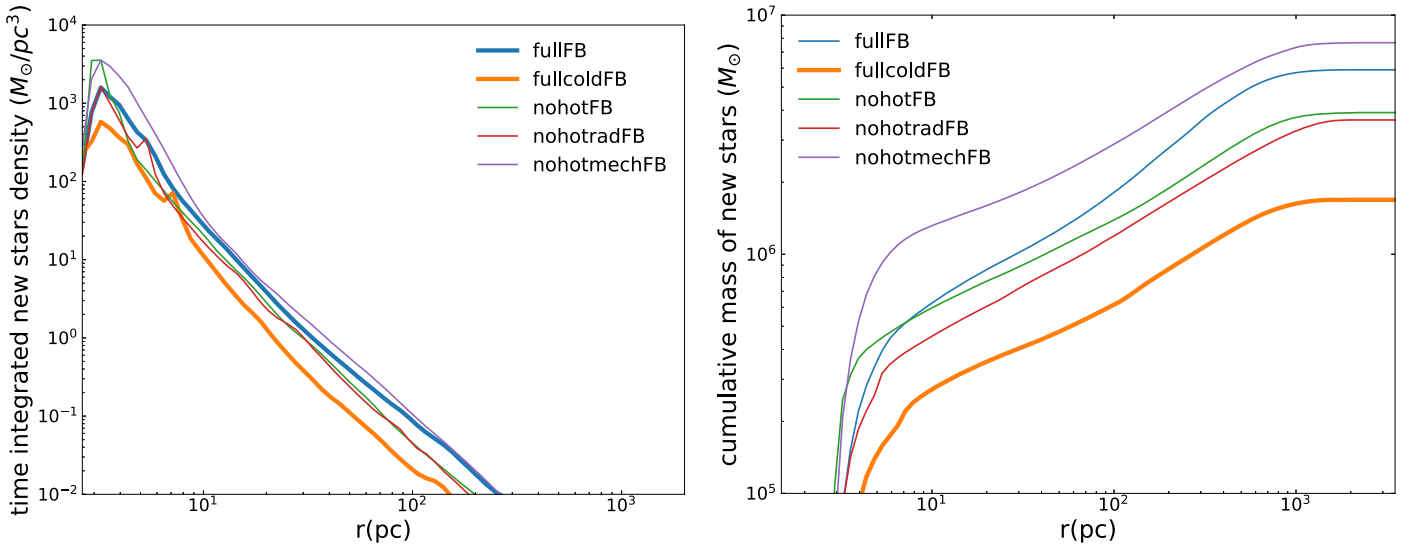


Figure 6. *Left:* the total mass of newly born stars at a given radius per unit volume. *Right:* the cumulative mass of the newly born stars.

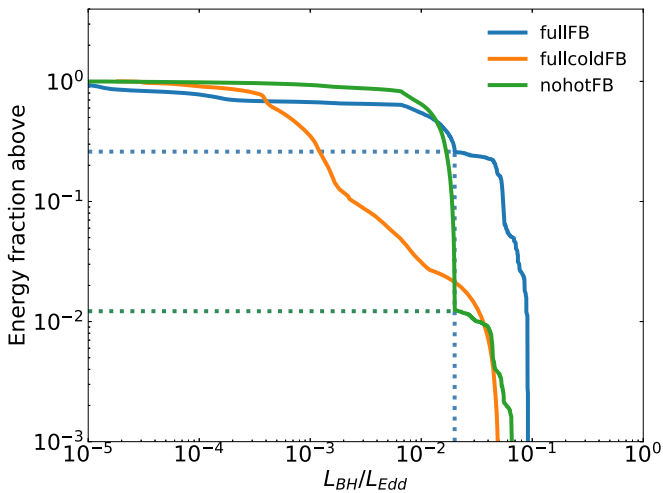


Figure 7. Percentage of the total cumulative energy emitted above the values of the Eddington ratios. The horizontal dotted lines represent the portion of emitted energy above the Eddington ratio of 0.02.

4. Summary and Conclusion

Recently we have continued our study of the effects of AGN feedback in an isolated elliptical galaxy (Li et al. 2018; Yoon et al. 2018; Yuan et al. 2018b; Gan et al. 2019), along the line of our previous works (e.g., Ciotti & Ostriker 2001, 2007; Ciotti et al. 2010; Gan et al. 2014). The main improvement of this series of works is the incorporation of state-of-the-art physics of black hole accretion in the model, including the exact discrimination of the hot and cold accretion modes and, more important, the recent important progress in our understanding of radiation and wind in the hot accretion mode. The adopted accretion physics has been presented in detail in Yuan18 (see also Yuan et al. 2018a). These works have focused on different aspects of the problem: low specific angular momentum galaxy (Yuan18), high specific angular momentum galaxy (Yoon et al. 2018), the different roles of AGN and stellar feedback (Li et al. 2018), and the role of gravitational instability of the gaseous disk (Gan et al. 2019).

While consensus has been reached that the accretion rate of the central black hole covers a wide range and the AGNs in most galaxies pass through both cold and hot modes during

their evolution, most previous work in this field focuses only on one mode; or even if they include both, the accretion physics is not correctly adopted. The aim of the present work is to study how important it is to correctly include both modes. For this aim, we specifically focus on the wind and radiation feedback in the hot mode (but the jet is neglected in this work).

We have run two test models, namely the fullcoldFB model and the nohotFB model (see Table 1). In the fullcoldFB model, the AGN always stays in the cold mode, no matter what value the accretion rate is. In the nohotFB model, we simply turn off the AGN feedback once the accretion rate is smaller than $0.2L_{\text{Edd}}/c^2$ (i.e., the AGN enters into the hot mode). We then compare the simulation results, such as AGN light curve and star formation, of these two models with the fullFB model, in which both modes are correctly included.

For the fullcoldFB model, the wind and radiation outputs from the AGN are in general much stronger than in the fullFB model (the left panel of Figure 1). These strong winds push the gas away from the black hole and even out of the galaxy. Consequently, the luminosity of the AGN becomes significantly lower and decreases with time (Figure 3). Because the AGN rarely stays in the high-luminosity regime in the fullcoldFB model, the percentage of the emitted total energy in the luminous regime becomes much smaller compared with the fullFB model, inconsistent with observational constraints (Figure 7). The stronger radiation in the fullcoldFB model also makes the thermal instability of the gas in the host galaxy harder to occur, and thus fewer clumps will be formed and the AGN light curve is less bursty compared with the fullFB model (Figure 3). The strong wind and radiation in the fullcoldFB model also strongly suppress the star formation in the host galaxy, so the total mass of newly born stars becomes an order of magnitude smaller compared with the fullFB model (Figure 6). This is because the strong winds blow the gas far away from the central region of the galaxy and the strong radiation also heats the gas in a large region of the galaxy.

For the nohotFB model, the AGN luminosity on average becomes significantly higher compared with the fullFB model. This is because the density of the gas surrounding the black hole becomes higher and temperature becomes lower due to the absence of the wind and radiation when the AGN accretion rate

is below $0.2L_{\text{Edd}}/c^2$. In accordance with this change, the black hole mass also becomes higher in the nohotFB model (Figure 5). It is interesting to note that, compared with the fullFB model, in the nohotFB model star formation is enhanced only at $r \leq 4$ pc, but is reduced in all the region beyond that radius. We speculate that the reason is that the power of wind in the hot mode is weak. In this case, winds are only able to blow the gas in the central region of the galaxy away. Beyond that radius, they mainly play a role of disturbing the gas and making the gas inhomogeneous, which is helpful for star formation.

In addition to the fullcoldFB and nohotFB models, we have also run two additional models, namely nohotradFB and nohotmechFB models (Table 1), to examine the respective roles of wind and radiation in the hot feedback mode. It is found that the overall results of the nohotradFB model are similar to the fullFB model, which implies that wind rather than radiation plays a dominant role in the hot feedback mode. This is further confirmed by the comparison between nohotmechFB and nohotFB models, which shows that their AGN light curve and star formation activity are similar. However, we find that the black hole growth is more suppressed in the nohotmechFB model compared with the nohotFB model, which is because of the additional radiative heating in the nohotmechFB model causing a decrease of the accretion rate. This indicates that, depending on the problem of our interest, radiation sometimes also plays an important role. Combined with Yuan18, this paper has found that the wind feedback dominates for controlling the black hole growth and the star formation activity, but the effect of radiative feedback is not negligible.

These results indicate that the hot mode plays an important role in AGN feedback and thus cannot be neglected; it is crucial to correctly include both modes.

Some caveats exist in the present work and we plan to investigate them in the future: (1) we only consider the low angular momentum galaxy; (2) we have not taken into account the external gas supply to the galaxy; (3) the jet is neglected; (4) dust has not been included. The quantitative results may change after we take into account these effects, but we expect that the major conclusions of the present paper should remain unchanged.

We are grateful to the referee for the constructive comments that have significantly improved our paper. We thank Drs. Yuan Li and Miao Li for useful discussions. D.Y. and F.Y. are supported in part by the National Key Research and Development Program of China (grant No. 2016YFA0400704), the Natural Science Foundation of China (grants 11573051, 11633006, 11650110427, 11661161012), the Key Research Program of Frontier Sciences of CAS (No. QYZDJSSW-SYS008), and the Astronomical Big Data Joint Research Center co-founded by the National Astronomical Observatories, Chinese Academy of Sciences, and the Alibaba Cloud. This work made use of the High Performance Computing Resource in the Core Facility for Advanced Research Computing at Shanghai Astronomical Observatory.

ORCID iDs

Doosoo Yoon  <https://orcid.org/0000-0001-8694-8166>

Feng Yuan  <https://orcid.org/0000-0003-3564-6437>

Jeremiah P. Ostriker  <https://orcid.org/0000-0002-6405-9904>

Luca Ciotti  <https://orcid.org/0000-0002-5708-5274>

References

- Arav, N., Moe, M., Costantini, E., et al. 2008, *ApJ*, 681, 954
- Blaes, O. 2014, *SSRv*, 183, 21
- Bower, R. G., Benson, A. J., Malbon, R., et al. 2006, *MNRAS*, 370, 645
- Bu, D.-F., & Mosallanezhad, A. 2018, *A&A*, 615, 35
- Bu, D.-F., Yuan, F., Gan, Z.-M., & Yang, X.-H. 2016a, *ApJ*, 818, 83
- Bu, D.-F., Yuan, F., Gan, Z.-M., & Yang, X.-H. 2016b, *ApJ*, 823, 90
- Cheung, E., Bundy, K., Cappellari, M., et al. 2016, *Natur*, 533, 504
- Ciotti, L., Morganti, L., & de Zeeuw, P. T. 2009a, *MNRAS*, 393, 491
- Ciotti, L., & Ostriker, J. P. 1997, *ApJL*, 487, L105
- Ciotti, L., & Ostriker, J. P. 2001, *ApJ*, 551, 131
- Ciotti, L., & Ostriker, J. P. 2007, *ApJ*, 665, 1038
- Ciotti, L., & Ostriker, J. P. 2012, in *Hot Interstellar Matter in Elliptical Galaxies*, Astrophysics and Space Science Library, 378, ed. D.-W. Kim & S. Pellegrini (Berlin: Springer), 83
- Ciotti, L., Ostriker, J. P., & Proga, D. 2009b, *ApJ*, 699, 89
- Ciotti, L., Ostriker, J. P., & Proga, D. 2010, *ApJ*, 717, 708
- Ciotti, L., & Pellegrini, S. 2017, *ApJ*, 848, 29
- Ciotti, L., & Pellegrini, S. 2018, *ApJ*, 868, 91
- Ciotti, L., Pellegrini, S., Negri, A., & Ostriker, J. P. 2017, *ApJ*, 835, 15
- Cisternas, M., Jahnke, K., Inskip, K. J., et al. 2011, *ApJ*, 726, 57
- Crenshaw, D. M., Kraemer, S. B., & George, I. M. 2003, *ARA&A*, 41, 117
- Cresci, G., Mainieri, V., Brusa, M., et al. 2015, *ApJ*, 799, 82
- Croton, D. J., Springel, V., White, S. D. M., et al. 2006, *MNRAS*, 365, 11
- Czoske, O., Barnabè, M., Koopmans, L. V. E., Treu, T., & Bolton, A. S. 2008, *MNRAS*, 384, 987
- Di Matteo, T., Springel, V., & Hernquist, L. 2005, *Natur*, 433, 604
- Dye, S., Evans, N. W., Belokurov, V., Warren, S. J., & Hewett, P. 2008, *MNRAS*, 388, 384
- Fabian, A. C. 2012, *ARA&A*, 50, 455
- Falceta-Gonçalves, D., Caproni, A., Abraham, Z., Teixeira, D. M., & de Gouveia Dal Pino, E. M. 2010, *ApJL*, 713, L74
- Fan, L., Fang, G., Chen, Y., et al. 2014, *ApJL*, 784, L9
- Gan, Z., Ciotti, L., Ostriker, J. P., & Yuan, F. 2019, *ApJ*, 872, 167
- Gan, Z., Yuan, F., Ostriker, J. P., Ciotti, L., & Novak, G. S. 2014, *ApJ*, 789, 150
- Gaspari, M., Ruszkowski, M., & Oh, S. P. 2013, *MNRAS*, 432, 3401
- Gofford, J., Reeves, J. N., McLaughlin, D. E., et al. 2015, *MNRAS*, 451, 4169
- Greene, J. E., & Ho, L. C. 2007, *ApJ*, 667, 131
- Guo, F. 2016, *ApJ*, 826, 17
- Guo, F., Duan, X., & Yuan, Y.-F. 2018, *MNRAS*, 473, 1332
- Habouzit, M., Genel, S., Somerville, R. S., et al. 2019, *MNRAS*, 484, 4413
- Haiman, Z., & Hui, L. 2001, *ApJ*, 547, 27
- Hayes, J. C., Norman, M. L., Fiedler, R. A., et al. 2006, *ApJS*, 165, 188
- Heckman, T. M., Kauffmann, G., Brinchmann, J., et al. 2004, *ApJ*, 613, 109
- Hirschmann, M., Dolag, K., Saro, A., et al. 2014, *MNRAS*, 442, 2304
- Homan, J., Neilsen, J., Allen, J. L., et al. 2016, *ApJL*, 830, L5
- Hopkins, P. F., Hernquist, L., Cox, T. J., & Kereš, D. 2008, *ApJS*, 175, 356
- Hopkins, P. F., Torrey, P., Faucher-Giguère, C.-A., Quataert, E., & Murray, N. 2016, *MNRAS*, 458, 816
- Jaffe, W. 1983, *MNRAS*, 202, 995
- Kauffmann, G., & Heckman, T. M. 2009, *MNRAS*, 397, 135
- King, A., & Pounds, K. 2015, *ARA&A*, 53, 115
- Kocevski, D. D., Faber, S. M., Mozena, M., et al. 2012, *ApJ*, 744, 148
- Kormendy, J., & Ho, L. C. 2013, *ARA&A*, 51, 511
- Li, J., Ostriker, J., & Sunyaev, R. 2013, *ApJ*, 767, 105
- Li, Y., & Bryan, G. L. 2014, *ApJ*, 789, 54
- Li, Y., Bryan, G. L., Ruszkowski, M., et al. 2015, *ApJ*, 811, 73
- Li, Y.-P., Yuan, F., Mo, H., et al. 2018, *ApJ*, 866, 70
- Ma, R.-Y., Roberts, S. R., Li, Y.-P., & Wang, Q. D. 2018, *MNRAS*, 483, 5614
- Magorrian, J., Tremaine, S., Richstone, D., et al. 1998, *AJ*, 115, 2285
- McAlpine, S., Bower, R. G., Harrison, C. M., et al. 2017, *MNRAS*, 468, 3395
- McClintock, J. E., & Remillard, R. A. 2006, in *Black Hole Binaries*, ed. W. H. G. Lewin & M. van der Klis (Cambridge: Cambridge Univ. Press), 157
- McCourt, M., Sharma, P., Quataert, E., & Parrish, I. J. 2012, *MNRAS*, 419, 3319
- McNamaras, B. R., & Nulsen, P. E. J. 2012, *NJPh*, 14, 055023
- Mihos, J. C., & Hernquist, L. 1996, *ApJ*, 464, 641
- Mosallanezhad, A., Bu, D., & Yuan, F. 2016, *MNRAS*, 456, 2877
- Mou, G., Yuan, F., Bu, D., Sun, M., & Su, M. 2014, *ApJ*, 790, 109
- Mou, G., Yuan, F., Gan, Z., & Sun, M. 2015, *ApJ*, 811, 37
- Murray, N., Quataert, E., & Thompson, T. A. 2005, *ApJ*, 618, 569
- Naab, T., & Ostriker, J. P. 2017, *ARA&A*, 55, 59

- Narayan, R., Sądowski, A., Penna, R. F., & Kulkarni, A. K. 2012, *MNRAS*, **426**, 3241
- Narayan, R., & Yi, I. 1995, *ApJ*, **452**, 710
- Negri, A., & Volonteri, M. 2017, *MNRAS*, **467**, 3475
- Novak, G. S., Ostriker, J. P., & Ciotti, L. 2011, *ApJ*, **737**, 26
- Novak, G. S., Ostriker, J. P., & Ciotti, L. 2012, *MNRAS*, **427**, 2734
- Ostriker, J. P., Choi, E., Ciotti, L., Novak, G. S., & Proga, D. 2010, *ApJ*, **722**, 642
- Pellegrini, S. 2012, in *Hot Interstellar Matter in Elliptical Galaxies*, Astrophysics and Space Science Library, 378, ed. D.-W. Kim & S. Pellegrini (Berlin: Springer), 21
- Pringle, J. E. 1981, *ARA&A*, **19**, 137
- Qiu, Y., Bogdanovic, T., Li, Y., Park, K., & Wise, J. H. 2019, *ApJ*, **877**, 47
- Rusin, D., & Kochanek, C. S. 2005, *ApJ*, **623**, 666
- Sazonov, S. Y., Ostriker, J. P., Ciotti, L., & Sunyaev, R. A. 2005, *MNRAS*, **358**, 168
- Sazonov, S. Y., Ostriker, J. P., & Sunyaev, R. A. 2004, *MNRAS*, **347**, 144
- Sądowski, A., Narayan, R., Penna, R., & Zhu, Y. 2013, *MNRAS*, **436**, 3856
- Schaye, J., Crain, R. A., Bower, R. G., et al. 2015, *MNRAS*, **446**, 521
- Shakura, N. I., & Sunyaev, R. A. 1973, *A&A*, **24**, 337
- Shankar, F., Croce, M., Miralda-Escudé, J., Fosalba, P., & Weinberg, D. H. 2010, *ApJ*, **718**, 231
- Sharma, P., McCourt, M., Quataert, E., & Parrish, I. J. 2012, *MNRAS*, **420**, 3174
- Sijacki, D., Springel, V., Di Matteo, T., & Hernquist, L. 2007, *MNRAS*, **380**, 877
- Soltan, A. 1982, *MNRAS*, **200**, 115
- Springel, V., Di Matteo, T., & Hernquist, L. 2005, *MNRAS*, **361**, 776
- Stone, J., Pringle, J. E., & Beleman, M. 1999, *MNRAS*, **310**, 1002
- Tadaki, K., Iono, D., Yun, M. S., et al. 2018, *Natur*, **560**, 613
- Tombesi, F., Cappi, M., Reeves, J. N., & Braitto, V. 2012, *MNRAS*, **422**, L1
- Tombesi, F., Tazaki, F., Mushotzky, R. F., et al. 2014, *MNRAS*, **443**, 2154
- Tremaine, S., Gebhardt, K., Bender, R., et al. 2002, *ApJ*, **574**, 740
- Vernaleo, J. C., & Reynolds, C. S. 2006, *ApJ*, **645**, 83
- Wang, C., Li, Y., & Ruszkowski, M. 2019, *MNRAS*, **482**, 3576
- Wang, Q. D., Nowak, M. A., Markoff, S. B., et al. 2013, *Sci*, **341**, 981
- Weinberger, R., Springel, V., Hernquist, L., et al. 2017, *MNRAS*, **465**, 3291
- Weinberger, R., Springel, V., Pakmor, R., et al. 2018, *MNRAS*, **479**, 4056
- Xie, F.-G., & Yuan, F. 2012, *MNRAS*, **427**, 1580
- Xie, F.-G., Yuan, F., & Ho, L. C. 2017, *ApJ*, **844**, 42
- Yoon, D., Yuan, F., Gan, Z.-M., et al. 2018, *ApJ*, **864**, 6
- Yu, Q., & Tremaine, S. 2002, *MNRAS*, **335**, 965
- Yuan, F., Bu, D., & Wu, M. 2012a, *ApJ*, **761**, 130
- Yuan, F., Gan, Z., Narayan, R., et al. 2015, *ApJ*, **804**, 101
- Yuan, F., & Narayan, R. 2014, *ARA&A*, **52**, 529
- Yuan, F., Ostriker, J. P., Yoon, D., et al. 2018a, arXiv:1807.05488
- Yuan, F., Wu, M., & Bu, D. 2012b, *ApJ*, **761**, 129
- Yuan, F., Yoon, D., Li, Y.-P., et al. 2018b, *ApJ*, **857**, 121